

# Calculation of the biquadratic spin interactions based on the spin cluster expansion for *ab initio* tight-binding models

Tatsuto Hatanaka<sup>1,2,\*</sup>, Juba Bouaziz<sup>3,†</sup>, Takuya Nomoto<sup>4,‡</sup> and Ryotaro Arita<sup>2,3,§</sup>

<sup>1</sup> *Department of Applied Physics, The University of Tokyo, Bunkyo-ku, Tokyo, 113-8656, Japan*

<sup>2</sup> *RIKEN Center for Emergent Matter Science (CEMS), Wako 351-0198, Japan*

<sup>3</sup> *Department of Physics, The University of Tokyo, Bunkyo-ku, Tokyo, 113-0033, Japan*

<sup>4</sup> *Department of Physics, Tokyo Metropolitan University, Hachioji, Tokyo 192-0397, Japan*

(Dated: July 29, 2024)

We devise a calculation scheme using *ab initio* tight-binding Hamiltonians to evaluate biquadratic magnetic interactions. This approach relies on the spin cluster expansion combined with the disordered local moment (DLM) method, originally developed within the multiple scattering Korringa-Kohn-Rostoker method. Applying it to the two-orbital Hubbard model, we show that the evaluated DLM biquadratic interactions agree well with those obtained from the strongly correlated limit, demonstrating wide applicability of the method to various magnetic systems with large local moments. We then apply it to the *ab initio* tight-binding models for bcc Fe and fcc Ni; the resulting magnetic interactions align well with previous studies in the literature. The present approach offers a convenient *ab initio* path for evaluating biquadratic interactions and understanding the electronic mechanisms controlling them.

## I. INTRODUCTION

Recently, antiferromagnetic materials with nontrivial spin arrangements have attracted broad interest due to their unique properties, making them suitable for technological applications [1–3]. These complex spin configurations often arise from spin interactions beyond what the standard Heisenberg model accounts for [4]. For instance, the Dzyaloshinskii-Moriya (DM) interaction [5, 6], which originates from the spin-orbit coupling and inversion symmetry breaking, is well-known for inducing noncollinear chiral spin structures such as magnetic skyrmions [7, 8]. In addition, the biquadratic interaction, a direct extension of the bilinear Heisenberg interaction, is also essential in stabilizing such complex spin arrangements [9, 10]. The biquadratic interaction can drive the system to a non-collinear configuration even in the absence of the spin-orbit coupling, its effects on various spin systems have been extensively investigated from both theoretical and experimental perspectives [11–18].

In order to quantify the strength of the biquadratic interaction within a first principles framework, it is highly desirable to derive parameters of the spin Hamiltonian from realistic *ab initio* methods [19]. For challenging task, the infinitesimal rotation method or Liechtenstein-Katsnelson-Antropov-Gubanov (LKAG) method [20–22] is established as a commonly used approach to extract spin Hamiltonian parameters and has been successfully applied to several material classes, including 3*d*-transition metal, 4*f*-elements and transition metal oxides [19, 23–31]. The LKAG approach consists of mapping the energy variation of magnetic quantum systems due to an infinitesimal rotation onto a classical system with localized spins [20]. The relativistic extension of the LKAG approach gives access to the DM interaction and

two-ion anisotropy [32, 33]. The asymptotic behavior of the obtained pair exchange interactions obtained by the LKAG approach is well-understood for both the strongly correlated and itinerant limits[34].

The LKAG approach has nonetheless a few shortcomings: First, the band energy variation due to an infinitesimal rotation is mapped onto bilinear interactions incorporating contributions from spin interactions of a higher-order nature. Second, the method is based on a magnetically ordered reference state, which may lead to different results depending on the chosen reference state [35, 36]; hence, this approach is suitable for a local mapping [37]. We note that while extended methods have been proposed to compute higher-order or multi-spin interactions [38, 39], the reference state dependence issue remains present.

An alternative approach to determine the exchange parameters of the classical spin model consists of fitting the total energy dependence of multiple spin configurations [40, 41]. This method enables the self-consistent evaluation of arbitrary spin configurations through the application of magnetic constraining fields [42] and derives exchange parameters to arbitrary orders. The drawbacks of this technique are the necessity for large multiple-atom supercells to handle complex spin configurations, the high computational cost, and the accuracy of the fitting procedure, which may lead to spurious results when dealing with small magnetic interactions in the meV range.

A computationally efficient method that accesses the pair and higher-order magnetic interactions without the reference state dependence or supercell limitations is highly desirable. The relativistic disordered local moment (RDLM) [43–46], combined with the the spin cluster expansion (SCE) [47, 48], provides an SCE-RDLM scheme for a systematic evaluation of magnetic interactions of arbitrary order [49–55]. In the SCE approach, the energy surface of a classical spin system with frozen length is systematically expanded into spin clusters using a real spherical harmonics basis. The basis describes the magnetic orientations of the spin moments, and the expansion coefficients encode the magnetic interactions. The order of the basis function dictates the form of spin Hamil-

\* [hatanaka-tatsuto346@g.ecc.u-tokyo.ac.jp](mailto:hatanaka-tatsuto346@g.ecc.u-tokyo.ac.jp)

† [jbouaziz@g.ecc.u-tokyo.ac.jp](mailto:jbouaziz@g.ecc.u-tokyo.ac.jp)

‡ [tnomoto@tmu.ac.jp](mailto:tnomoto@tmu.ac.jp)

§ [arita@riken.jp](mailto:arita@riken.jp)

tonian [47]. Lastly, considering the paramagnetic state in the DLM picture for this approach is essentially free from the reference state dependence

The SCE-RDLM scheme was originally formulated for the multiple scattering theory based on the Green's function methods, such as the Korringa-Kohn-Rostoker (KKR) method [56], and implemented in the spin density functional theory (SDFT). In this work, we formulate the scheme for *ab initio* tight-binding models. Our method relies on commonly available plane wave codes [57] and is applicable to magnetic material classes with large local moments independently from the basis of first-principles calculations. The presented approach is a useful tool to understand and predict the physical properties of magnetic materials with complex spin configurations that arise from higher-order spin interactions.

The paper is structured as follows: In Section II, we formulate SCE-DLM, the nonrelativistic version of SCE-RDLM, for *ab initio* tight-binding models. The presented approach is applicable to arbitrary spin interactions, our primary emphasis is on the biquadratic exchange interaction, which plays a central role in stabilizing non-coplanar order in antiferromagnets without the assistance of relativistic effects (DM interaction). The computational details and setups are present in Section III. Section IV is dedicated to the benchmarking and validation of our approach: we apply it to the one-dimensional two-orbital Hubbard model. We analyze the asymptotic behavior of the bilinear and biquadratic interactions calculated for the limit of strong correlation and confirm that the interactions evaluated by SCE-DLM align with those evaluated for the effective quantum spin model. Next, we apply the SCE-DLM to two prototypical transition metal magnets, namely bcc Fe and fcc Ni, and show the results obtained with the *ab initio* tight-binding approach. We then compare our results with the ones obtained using the KKR method and previous theoretical ones on the biquadratic interaction for bcc Fe and fcc Ni in V. Finally, in Section VI, we conclude and summarize our work.

## II. FORMULATION

### A. Spin Cluster Expansion

The spin cluster expansion (SCE) developed by Drautz and Fähnle [47, 48] provides a tool to expand systematically the energy of a many-body classical spin system by introducing clusters consisting of several spins. The SCE employs a complete orthonormal basis set, namely the real spherical harmonics  $Y_{L=(l,m)}(\mathbf{e})$  for a unit vector  $\mathbf{e}$  of a classical spin. The basis functions for a cluster  $C$  are built from a multiplication of the basis functions of every single spin resulting in:

$$\Phi_C^{\{L\}}(\{\mathbf{e}\}) = \frac{1}{(4\pi)^{(N-n)/2}} \prod_{i \in C} Y_{L_i}(e_i) \quad (1)$$

where  $N$  refers to the number of all spins in the system,  $n$  indicates the size of the cluster,  $\{\mathbf{e}\}$  is an array that represents the spin directions, and  $\{L\}$  is an array containing the combined orbital index  $L = (l, m)$  of each spin in the cluster  $C$ .

These basis functions of the clusters also form a complete and orthonormal basis. The grand potential of the spin system can then be expanded in terms of the cluster basis as:

$$\Omega(\{\mathbf{e}\}) = \Omega_0 + \sum_C \sum_{\{L\}} J_C^{\{L\}} \Phi_C^{\{L\}}(\{\mathbf{e}\}) \quad (2)$$

where the expansion coefficients of each cluster are defined as:

$$J_C^{\{L\}} = \langle \Phi_C^{\{L\}} | \Omega \rangle \quad (3)$$

$$\langle f | g \rangle = \int \cdots \int \left[ \prod_{i=1}^N (d^2 e_i) \right] f(\{\mathbf{e}\}) g(\{\mathbf{e}\}) \quad (4)$$

where  $\Omega_0$  and  $\int d^2 e$  stand for a constant offset independent of the spin configuration and integration over the surface of a unit sphere, respectively. In Eq. (3), we use the useful Dirac bracket notation, and the inner product in this notation is defined in Eq. (4) for functions  $f$  and  $g$  which depend on the spin configuration  $\{\mathbf{e}\}$ .

Our focus lies in two site interactions (pair and biquadratic). Therefore, we consider the grand potential expanded up to the two-spin clusters. We note that the expansion for clusters consisting of multiple sites can be performed in a similar way:

$$\begin{aligned} \Omega(\{\mathbf{e}\}) = \Omega_0 + \sum_i \sum_{L \neq (0,0)} J_i^L Y_L(e_i) \\ + \frac{1}{2} \sum_{i \neq j} \sum_{L, L' \neq (0,0)} J_{ij}^{LL'} Y_L(e_i) Y_{L'}(e_j) \end{aligned} \quad (5)$$

Each expansion coefficient for one/two spin clusters can be evaluated using the inner product in Eqs. (3) and (4).

$$J_i^L = \int d^2 e_i \langle \Omega \rangle_{e_i} Y_L(e_i) \quad (6)$$

$$J_{ij}^{LL'} = \iint d^2 e_i d^2 e_j \langle \Omega \rangle_{e_i, e_j} Y_L(e_i) Y_{L'}(e_j) \quad (7)$$

$$\langle \Omega \rangle_C = \frac{1}{(4\pi)^{N-n}} \int \cdots \int \left[ \prod_{i \notin C} (d^2 e_i) \right] \Omega(\{\mathbf{e}\}) \quad (8)$$

where  $\langle \Omega \rangle_C$  stands for the expectation value calculated by integrating all solid angles except for spins in the cluster  $C$ . The directions of the spins outside the cluster are integrated over, and the evaluated coefficients are independent of a reference state. Since we can not straightforwardly calculate Eq. (8) for many-body systems, we use the disordered local moment state, which is discussed in Sec. II B.

### B. Disordered Local Moment

The coherent potential approximation (CPA) was initially introduced to compute the electronic structure of disordered alloys [58]. The CPA relies on embedding impurities described by a single site scattering matrix into an effective medium and imposing that the additional impurity scattering

should vanish. The disordered local moment (DLM) approach employs a similar approach to CPA to incorporate the effect of transverse spin fluctuation [43]. The DLM relies on the approximation that the local moments  $\{e\}$  motion is much slower than the electronic ones. The CPA averaging is done on the magnetic moment orientations and models an electronic structure in the paramagnetic state with randomly oriented spins. While the DLM method was originally developed for the KKR method, it can similarly be formulated for the tight-binding Hamiltonians [59].

Here, we consider the multi-orbital tight-binding Hamiltonian defined as:

$$\mathcal{H} = \sum_{i\ell\sigma, jm\sigma'} \left( H_{i\ell\sigma, jm\sigma'} \hat{c}_{i\ell\sigma}^\dagger \hat{c}_{jm\sigma'} + \text{h.c.} \right), \quad (9)$$

where  $(i, j)$ ,  $(\ell, m)$ , and  $(\sigma, \sigma')$  are the indices of sites, orbitals, and spins, respectively. The operator  $\hat{c}_{i\ell\sigma}/\hat{c}_{i\ell\sigma}^\dagger$  stands for the annihilation/creation operator of an electron specified with the degrees of freedom  $(i\ell\sigma)$ . We divide each component of the Hamiltonian into the spin-independent off-site hopping  $t$  and the on-site magnetic potential term  $v$ ,

$$H_{i\ell\sigma, jm\sigma'} = t_{i\ell, jm} \delta_{\sigma, \sigma'} + \delta_{ij} v_{\ell, m}^i [e_i \cdot \sigma]_{\sigma\sigma'}, \quad (10)$$

where  $e_i, \sigma$  is the direction of a spin at the site  $i$  and the Pauli matrix vector, respectively. Here, we assume that there are no spin-dependent hopping terms and that the spin-dependent potentials  $v$ 's are a local quantity. Although there could be non-local spin-dependent potentials in the tight-binding Hamiltonian constructed from first principles, the latter are not included to improve computational efficiency [22]. We denote the former term of Eq. (10) as  $H_0$  and the latter as  $V$  such that  $H = H_0 + V$ .

In the DLM method, we consider the virtual state with randomly oriented spins and introduce the self-energy  $\Sigma$ , instead of the spin-dependent potential  $V$ , corresponding to the effective potential of such a disordered state as follows:

$$H_c = H_0 + \Sigma \quad (11)$$

$$H = H_c + (V - \Sigma), \quad (12)$$

where  $H_c$  indicates the Hamiltonian of the DLM state. Note that the introduced self-energy  $\Sigma$  is a local and spin-independent complex quantity so that  $\Sigma_{i\ell\sigma, jm\sigma'} = \delta_{ij} \delta_{\sigma\sigma'} \tilde{\Sigma}_{\ell\sigma, m\sigma'}^i$ . The Green's functions in the real space are given as follows:

$$\bar{G}(\epsilon) = [\epsilon - H_c]^{-1} \quad (13)$$

$$\begin{aligned} G(\epsilon) &= [\epsilon - H]^{-1} \\ &= \bar{G} [1 + \bar{G}(V - \Sigma)]^{-1}, \end{aligned} \quad (14)$$

We also introduce the scattering matrix  $T$  as follows:

$$T_i(e_i) = \left( V_i(e_i) - \tilde{\Sigma}^i \right) \left[ 1 - \bar{G}_{ii} \left[ V_i(e_i) - \tilde{\Sigma}^i \right] \right]^{-1} \quad (15)$$

where  $V_i(e_i)$  stands for the magnetic potential of the spin at site  $i$  with the orientation  $e_i$ , namely  $[V_i(e_i)]_{\ell\sigma, m\sigma'} =$

$v_{\ell, m}^i [e_i \cdot \sigma]_{\sigma\sigma'}$ , and the scattering matrix  $T_i(e_i)$  has the same degrees of freedom with those of  $V_i(e_i)$ . We then can formulate the CPA condition for the tight-binding Hamiltonian with the single-site approximation [59],

$$\frac{1}{4\pi} \int d^2 e_i T_i(e_i) = 0. \quad (16)$$

In the absence of the relativistic spin-orbit coupling (SOC), the CPA condition in Eq.(16) is expressed as follows (Ising DLM):

$$\frac{T_i(\hat{z}) + T_i(-\hat{z})}{2} = 0, \quad (17)$$

where  $\hat{z}$  is a unit vector along the  $z$ -axis.

In practice, we determine the self-energy and the chemical potential in a self-consistent manner [59]. The chemical potential  $\mu_c$  of the DLM state is set by the conservation condition for the number of electrons below,

$$N = -\frac{1}{\pi} \int d\epsilon f(\epsilon) \text{Im Tr } \bar{G}(\epsilon) \quad (18)$$

$$f(\epsilon) = \frac{1}{1 + e^{\beta(\epsilon - \mu_c)}} \quad (19)$$

where  $\text{Tr}$  stands for taking a trace over all indices of the sites, orbitals, and spins, and  $f(\epsilon)$  is the Fermi distribution function.

### C. SCE-DLM scheme

The restricted averages of the grand potential  $\langle \Omega \rangle_{e_i e_j}$  are the central quantities of interest to determine the two-site magnetic interactions [49].  $\langle \Omega \rangle_{e_i e_j}$  are obtained using the Lloyd's formula [60, 61] for the reference state, i.e., the DLM state. Within our tight-binding formulation, we obtain the following expression:

$$\begin{aligned} \langle \Omega \rangle_{e_i e_j} &= \Omega_0 - \frac{1}{\pi} \text{Im} \int d\epsilon f(\epsilon) \left[ \ln \det [1 + T_i(e_i) \bar{G}_{ii}] \right. \\ &\quad + \ln \det [1 + T_j(e_j) \bar{G}_{jj}] \\ &\quad + \sum_{l \neq i, j} \int d^2 e_l \ln \det [1 + T_l(e_l) \bar{G}_{ll}] \\ &\quad \left. + \sum_{k=1}^{\infty} \frac{1}{k} \text{Tr} \left[ (T_i(e_i) \bar{G}_{ij} T_j(e_j) \bar{G}_{ji})^k \right] \right] \end{aligned} \quad (20)$$

where  $\Omega_0$  stands for the energy of the DLM state. The second and third terms indicate the corrections in the integrated density of states from the DLM state due to fixing the orientations of spins in the cluster consisting of spin  $i$  and  $j$  corresponding to the orientations  $e_i$  and  $e_j$ . The fourth term takes into account the contributions of spins outside the cluster, integrated over spin directions via Eq. (8). The fifth term denotes the contributions from the scatterings within the two-spin cluster. The two site expansion coefficients are then obtained using

Eq. (7), the integration with the spherical harmonics yields the expansion coefficients for the two-spin clusters [49],

$$J_{ij}^{LL'} = -\frac{1}{\pi} \text{Im} \int d\epsilon f(\epsilon) \iint d^2\mathbf{e}_i d^2\mathbf{e}_j Y_L(\mathbf{e}_i) Y_{L'}(\mathbf{e}_j) \times \ln \det [1 - T_i(\mathbf{e}_i) \bar{G}_{ij} T_j(\mathbf{e}_j) \bar{G}_{ji}]. \quad (21)$$

In order to map the energy expanded with the one/two-spin clusters in Eq. (2) to the following classical spin Hamiltonian,

$$\mathcal{H} = -2 \sum_{\langle i,j \rangle} [J_{ij}(\mathbf{e}_i \cdot \mathbf{e}_j) + B_{ij}(\mathbf{e}_i \cdot \mathbf{e}_j)^2], \quad (22)$$

we use the sum rule for the spherical harmonics below,

$$\frac{4\pi}{2l+1} \sum_m Y_l^m(\mathbf{e}_i) Y_l^m(\mathbf{e}_j) = P_l(\mathbf{e}_i \cdot \mathbf{e}_j) \quad (23)$$

where  $P_l(x)$  is the Legendre polynomial. Here, we consider a SOC-free case, so that the Hamiltonian has the SU(2) symmetry. Hence, the expansion coefficients  $J_{ij}^{LL'}$  do not depend on  $m$ , i.e., the spin interactions are isotropic. Given that the bilinear and biquadratic interactions in the Hamiltonian in Eq. (22) correspond to  $l = 1$  and 2, respectively, we can obtain these parameters from the expansion coefficients  $J_{ij}^{LL'}$  as follows:

$$J_{ij} = \frac{1}{8\pi} \sum_{m=-1}^1 J_{ij}^{(1,m)(1,m)} = \frac{3}{8\pi} J_{ij}^{(1,0)(1,0)} \quad (24)$$

$$B_{ij} = \frac{3}{16\pi} \sum_{m=-2}^2 J_{ij}^{(2,m)(2,m)} = \frac{15}{16\pi} J_{ij}^{(2,0)(2,0)} \quad (25)$$

### III. COMPUTATIONAL DETAILS

#### A. SCE-DLM scheme

In the calculation, the inverse temperature  $\beta$  was set to 500 eV<sup>-1</sup>. To evaluate the Green's function in the reciprocal space, we use 256×1×1 and 24×24×24  $k$ -point grid for the one-dimensional Hubbard model and 3d transition metals, respectively. We employ the efficient Lebedev quadrature scheme [62] in the integration over solid angles. The integration over real energies in Eqs. (18) and (21) can be transformed to the summation over the fermionic Matsubara poles by analytical continuation. We use the intermediate representation of the Green's function [63, 64] to reduce the computational cost.

#### B. Construction of Wannier-based tight-binding model

We performed SDFT calculations for the 3d metals with the QUANTUM ESPRESSO package [65, 66] with non-relativistic pseudopotentials in PSLibrary [67]. We used the projector augmented wave method [68, 69] and the Perdew-Burke-Ernzerhof exchange-correlation functional [70]. The

energy cut-off for the plane-wave basis was set to 50 Ry, and a 16×16×16  $k$ -point grid was used. We set the lattice constant as the experimental value of  $a = 2.866 \text{ \AA}$  for bcc Fe and  $a = 3.524 \text{ \AA}$  for fcc Ni.

The Wannier functions were constructed using the Wannier90 code [71–74]. The inner window to reproduce the low energy band dispersion of the DFT calculations was set from  $E_F - 10$  to  $E_F + 10$  eV, with  $E_F$  being the Fermi energy. We constructed a nine-orbital model containing one 4s, five 3d, and three 4p atomic orbitals per atom. In constructing the Wannier functions, 8×8×8 sampling  $k$ -point grid was used. The present calculation employs the plane-wave basis, it should be noted that the construction of the tight-binding model does not depend on the choice of the basis functions of the SDFT calculation.

#### C. KKR method

In order to benchmark our *ab initio* tight-binding for BCC Fe, we performed SDFT calculations using the all-electron full-potential KKR Green function method using the jukkr code [75], in the scalar relativistic approximation and neglecting spin-orbit coupling. The cutoff of the orbital momentum expansion for the KKR Green function is set at  $l_{\max} = 3$ . The self-consistent calculations are performed using an energy contour including 51 energy points and a Fermi-Dirac smearing of 500 K with a k-mesh density of 30×30×30. The exchange correlation is included in the Generalized Gradient approximation (GGA) [76]. The paramagnetic (DLM) state is obtained using CPA approximation with 50% spin-up and down magnetic configurations, including charge self-consistency. The magnetic interactions are computed from the DLM reference state. The pair interactions are obtained using the infinitesimal rotation method [21]. The biquadratic interactions are computed via the fourth order extension of the infinitesimal rotation method [39] (as shown in Eq. (34)). The pair and biquadratic interactions are computed on an energy contour, which includes 128 energy points and a Fermi-Dirac smearing of 200 K and a 40×40×40 k-mesh.

### IV. RESULTS

#### A. Two-Orbital Hubbard model

Here, we first study the one-dimensional two-orbital Hubbard model with the nearest-neighbor hopping and intra-orbital Coulomb repulsion  $U$  considered in Ref. [77]. This model offers one of the simplest cases that exhibit the biquadratic interaction when deriving an effective quantum spin model. The Hamiltonian is defined as

$$\mathcal{H} = - \sum_{\langle i\ell, jm \rangle, \sigma} (t_{i\ell, jm} \hat{c}_{i\ell\sigma}^\dagger \hat{c}_{jm\sigma} + \text{h.c.}) + \sum_i U \hat{n}_{i\uparrow} \hat{n}_{i\downarrow} \quad (26)$$

where  $(i, j)$ ,  $(\ell, m)$  and  $\sigma$  are the degrees of freedom of sites, orbitals, and spin, respectively. The bracket  $\langle \rangle$  stands for

the summation of the combinations between nearest-neighbor sites.  $\hat{c}_{i\ell\sigma}/\hat{c}_{i\ell\sigma}^\dagger$  and  $\hat{n}_{i\sigma}$  are the annihilation/creation and number operator of an electron. We show the schematic picture of the model in Fig. 1.

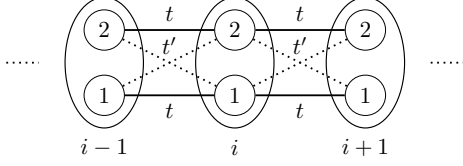


FIG. 1. One-dimensional two-orbital Hubbard model with the nearest neighbor hopping. The Hamiltonian has two types of transfer integrals,  $t$  and  $t'$ , defined for the pairs of orbitals shown with the solid and dashed lines, respectively.

The Hubbard Hamiltonian is defined using the spin-1/2 degree of freedom for each orbital, in the limit of strong correlation, we can derive an effective quantum spin model using the spin-1 degree of freedom for each site [77]:

$$\mathcal{H}_{\text{eff}} = -2 \left[ \sum_{\langle i,j \rangle} J_{ij}^{\text{Q}} (\hat{\mathbf{S}}_i \cdot \hat{\mathbf{S}}_j) + \sum_{\langle i,j \rangle} B_{ij}^{\text{Q}} (\hat{\mathbf{S}}_i \cdot \hat{\mathbf{S}}_j)^2 \right], \quad (27)$$

where the superscript Q denotes the interactions in the quantum spin model. The bilinear and biquadratic interactions can be obtained perturbatively as follows[77]:

$$J_{ij}^{\text{Q}} = -\frac{t^2 + t'^2}{U}, \quad B_{ij}^{\text{Q}} = -\frac{20t^2 t'^2}{U^3}. \quad (28)$$

Next, to compare the interactions in the quantum spin model with those in the classical spin model evaluated from SCE-DLM, denoted as  $J_{ij}^{\text{C}}$  and  $B_{ij}^{\text{C}}$ , respectively, we take the classical limit of the quantum spin [78]. For a  $S$ -spin length, the interactions need to be rescaled as follows [79]:

$$J_{ij}^{\text{Q}} (\hat{\mathbf{S}}_i \cdot \hat{\mathbf{S}}_j) \rightarrow S^2 J_{ij}^{\text{C}} (\mathbf{e}_i \cdot \mathbf{e}_j) \quad (29)$$

$$B_{ij}^{\text{Q}} (\hat{\mathbf{S}}_i \cdot \hat{\mathbf{S}}_j)^2 \rightarrow S^4 B_{ij}^{\text{C}} (\mathbf{e}_i \cdot \mathbf{e}_j)^2. \quad (30)$$

Hence, we compare  $J_{ij}^{\text{C}}$  with  $J_{ij}^{\text{Q}}$ , and likewise,  $B_{ij}^{\text{C}}$  with  $B_{ij}^{\text{Q}}$ , since we are examining the spin-1 case, where  $S = 1$ .

To apply SCE-DLM to this model, we first construct a tight-binding Hamiltonian including both the hopping parameter  $t$  and spin splitting  $B$ , which can be obtained via the mean-field approximation for the half-filled state of the Hamiltonian Eq. (26):

$$\mathcal{H}_{\text{MF}} = - \sum_{\langle i\ell, jm \rangle, \sigma} (t_{i\ell, jm} \hat{c}_{i\ell\sigma}^\dagger \hat{c}_{jm\sigma} + \text{h.c.}) - \mathbf{B}_i \cdot \hat{\mathbf{m}}_i \quad (31)$$

$$\mathbf{B}_i = \frac{U}{2} \langle \hat{\mathbf{m}}_i \rangle, \quad \hat{\mathbf{m}}_i = \sum_{\ell, \sigma, \sigma'} \hat{c}_{i\ell\sigma}^\dagger \boldsymbol{\sigma} \hat{c}_{i\ell\sigma'} \quad (32)$$

For the half-filled case with  $t \ll U$ , the magnetization operator  $\hat{\mathbf{m}}_i$  becomes  $\sigma_z \hat{z}$ . Consequently, we can obtain the Hubbard parameter  $U$  from the magnitude of the spin splitting  $B = |\mathbf{B}|$ , i.e.,  $U = 2B$ .

In Fig. 2, we plot  $J_{ij}^{\text{C}}, J_{ij}^{\text{Q}}, B_{ij}^{\text{C}}, B_{ij}^{\text{Q}}$  for the half-filled case as a function of  $t/U$ . It is worth noting that the chemical potential  $\mu_c$  of the DLM state is always zero for the half-filled state. We can see that the interactions evaluated perturbatively for the quantum spin model align closely with those derived from SCE-DLM in the limit of  $t/U \rightarrow 0$ . This result suggests that the present method is applicable to a wide variety of strongly correlated magnetic compounds with a strong local moment.

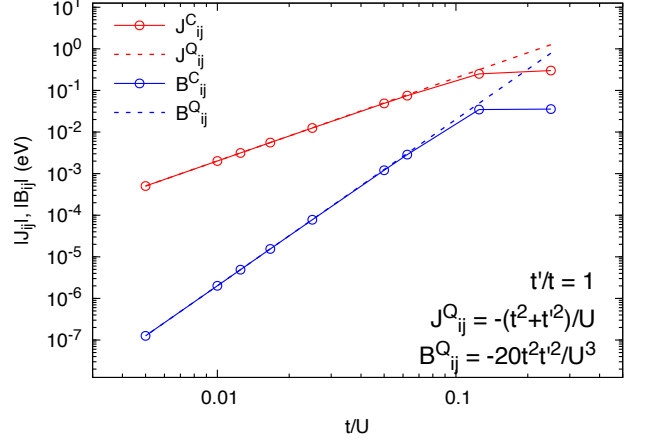


FIG. 2. Bilinear ( $J_{ij}^{\text{C}}/J_{ij}^{\text{Q}}$ ) and biquadratic ( $B_{ij}^{\text{C}}/B_{ij}^{\text{Q}}$ ) interactions in the classical/quantum spin Hamiltonian for  $t = t'$  in the limit of strong correlation  $t \ll U$ .  $J_{ij}^{\text{C}}$  (solid red line) and  $B_{ij}^{\text{C}}$  (solid blue line) are evaluated by SCE-DLM, and  $J_{ij}^{\text{Q}}$  (dashed red line) and  $B_{ij}^{\text{Q}}$  (dashed blue line) are evaluated perturbatively (see Eq. (28)).

## B. 3d transition metals

Next, we apply our scheme to the *ab initio* tight-binding models for the prototypical magnetic metals, bcc Fe and fcc Ni. In Fig. 3, we present the band structures of bcc Fe and fcc Ni obtained by SDFT calculations and those fitted by the Wannier-based tight-binding model.

In Fig. 4, we show the density of states (DOS) and integrated DOS along with the calibrated chemical potential  $\mu_c$  for the DLM state. Let us now compare the chemical potential ( $\mu$ ) and magnetic moment of the DLM and ferromagnetic (FM) state. Following the procedure outlined in Refs. [59, 80], we calculated the DOS for each spin component of the DLM state using the Green's function:

$$\overline{G}_{ii}^{\sigma\sigma} = \overline{G}_{ii} + \overline{G}_{ii} T_i(\sigma \hat{z}) \overline{G}_{ii}. \quad (33)$$

$\mu_c$ , the chemical potential of the DLM state measured from that of the FM state, is 0.55 eV for bcc Fe and -0.15 eV for fcc Ni. Namely,  $\mu$  of bcc Fe depends more sensitively on the changes in the electronic/magnetic structure compared to fcc Ni. Regarding the magnetic moment, which is defined as the difference in the number of the spin-up and spin-down electrons up to the chemical potential, for bcc Fe, it is 2.27

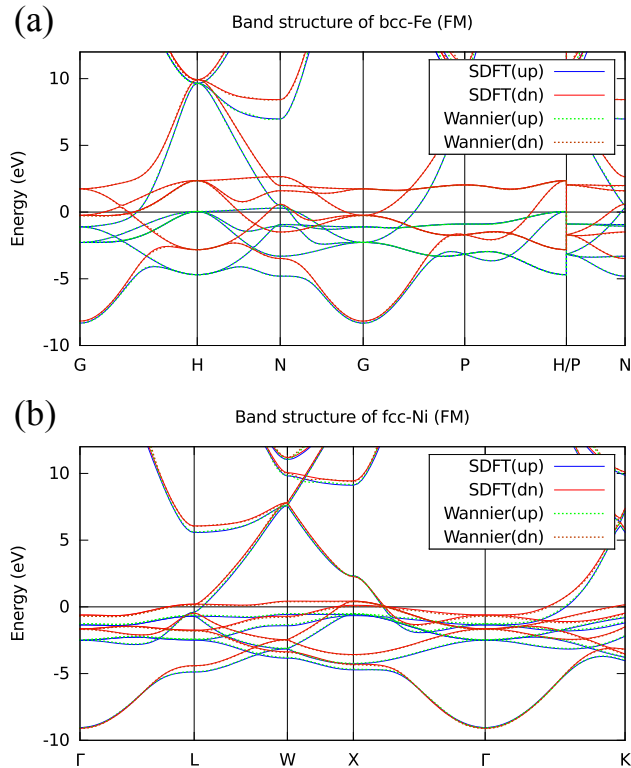


FIG. 3. Band structure of (a) bcc Fe and (b) fcc Ni. Blue and red lines are those for the up and down spin components obtained by SDFT calculation, and green and orange lines are those obtained by Wannier interpolation.

(2.28)  $\mu_B$  for the FM (DLM) state. For fcc Ni, it is 0.66 (0.48)  $\mu_B$  for the FM (DLM) state.

To verify the validity of these results, we compare the DLM state for bcc Fe obtained by the *ab initio* tight-binding (TB) method and that calculated by the KKR method. In the KKR calculation, the magnetic moment is calculated to be 2.21 (2.18)  $\mu_B$  for the FM (DLM) state, and the Fermi energy of the DLM state relative to the FM state is 0.33 eV. Similar to the result for the TB model, while the magnitude of the magnetic moment hardly depends on the magnetic states, the Fermi energies for the FM and DLM states are quite different. In Fig. 5, we compare the density of states of the DLM state obtained using KKR method with that in Fig. 4 (a). Note that the energy axis in Fig. 5 is adjusted by subtracting  $\mu_c$  for each method. We see that these two methods give almost the same density of states.

We then evaluate the nearest-neighbor (NN) bilinear ( $J$ ) and biquadratic ( $B$ ) interactions by SCE-DLM. In Fig. 6, we plot  $J$  and  $B$  as a function of the chemical potential  $\mu$ . For  $J$ , we compare the result with that obtained by the LKAG approach. We here define  $\mu_{\text{FM}} = \mu$  for the LKAG approach and  $\mu_{\text{DLM}} = \mu - \mu_c$  for the SCE-DLM approach. It can be seen that the dependence on  $\mu_{\text{FM}}$  in LKAG and the dependence on  $\mu_{\text{DLM}}$  in SCE-DLM are similar. It should be noted that this  $\mu_{\text{FM}}$  dependence in the LKAG qualitatively explains the magnetism observed in 3d transition metals [23]. Regarding  $B$ ,

we see that its energy scale is much smaller than that of  $J$  since it is a higher order interaction involving more scattering processes.  $B$  shows many sign changes as a function of  $\mu_{\text{DLM}}$ , it is negative at  $\mu_{\text{DLM}} = 0$  for both bcc Fe and fcc Ni.

In Fig. 7, we plot the bilinear ( $J_{ij}$ ) and biquadratic ( $B_{ij}$ ) interactions as a function of the distance ( $R$ ) between the  $i$ -th and  $j$ -th site for the range of  $-0.1 \leq \mu_{\text{FM/DLM}} \leq 0.1$  for both LKAG and SCE-DLM methods. From Fig. 7(a), (b), (d), and (e), we see that the  $\mu_{\text{FM(DLM)}}$  dependence around  $\mu_{\text{FM(DLM)}} = 0$  of the NN interaction  $J$  is significant for bcc Fe (fcc Ni) in the LKAG (SCE-DLM) calculation, which could cause sizable computational errors in the evaluation of  $J$ . In addition, we observe the following from Fig. 7: (a, b) For bcc Fe, the second NN interaction calculated by LKAG is as large as the NN interaction, the one calculated by SCE-DLM is negligibly small. These features align with the results using the KKR method as shown in Fig. 8 (a). In Fig. 7 (c), for bcc Fe, the size of the second NN  $B_{ij}$  is as large as that of the NN interaction, which also aligns with the results of the approach based on fitting the spin-configuration dependence of the total energy [81]. The  $\mu_{\text{DLM}}$  dependence of the NN interaction  $\mu_{\text{DLM}}$  of  $B_{ij}$  for the NN interaction is weak while the second NN neighbour changes considerably.

In Figs. 8 (a) and (b), we show the results of  $J_{ij}$  and  $B_{ij}$  as a function of the distance  $R$  between sites  $i$  and  $j$  at  $\mu_{\text{FM/DLM}} = 0$  for bcc Fe. We compare the magnetic interactions evaluated by the four methods: (1) LKAG for the TB model, (2) LKAG within the KKR scheme, (3) SCE-DLM for the TB model, and (4) the local force approach for the DLM state within the KKR scheme. On the one hand, for the LKAG methods (method (1) and (2)), the computed  $J_{ij}$ 's differ by about 5 meV, which can be attributed to the dependence on the implementation details [19], and the strong dependence on the chemical potential (as shown Fig 7). On the other hand,  $J_{ij}$  evaluated employing the DLM-based methods (method (3) and method (4)) closely agree with each other up to the long-range limit. In addition, the biquadratic interactions ( $B_{ij}$ ) computed using the two DLM-based approaches (method (3) and method (4)) are very close. For bcc Fe in the DLM state, the dependence on the chemical potential is weak, resulting in a better agreement between the TB and KKR methods.

## V. DISCUSSION

A variety of methods to calculate the biquadratic interaction from first principles have been proposed. So far, theoretical calculations for bcc Fe have yielded both positive[39, 82] and negative values[38, 81, 83–85] for the NN biquadratic interaction. Though all results for fcc Ni consistently show negative values[38, 39], there are fewer studies compared to bcc Fe. Aside from Refs. [81, 82], these works are based on LKAG and rely on the FM reference state to evaluate the biquadratic interaction. Our SCE-DLM approach differs from such approaches in that we need no ordered reference state. As is outlined in Ref. [86], approaches with a magnetically ordered state are valid for calculating physical properties related to the specific ordered state, such as the magnon spectrum [38].

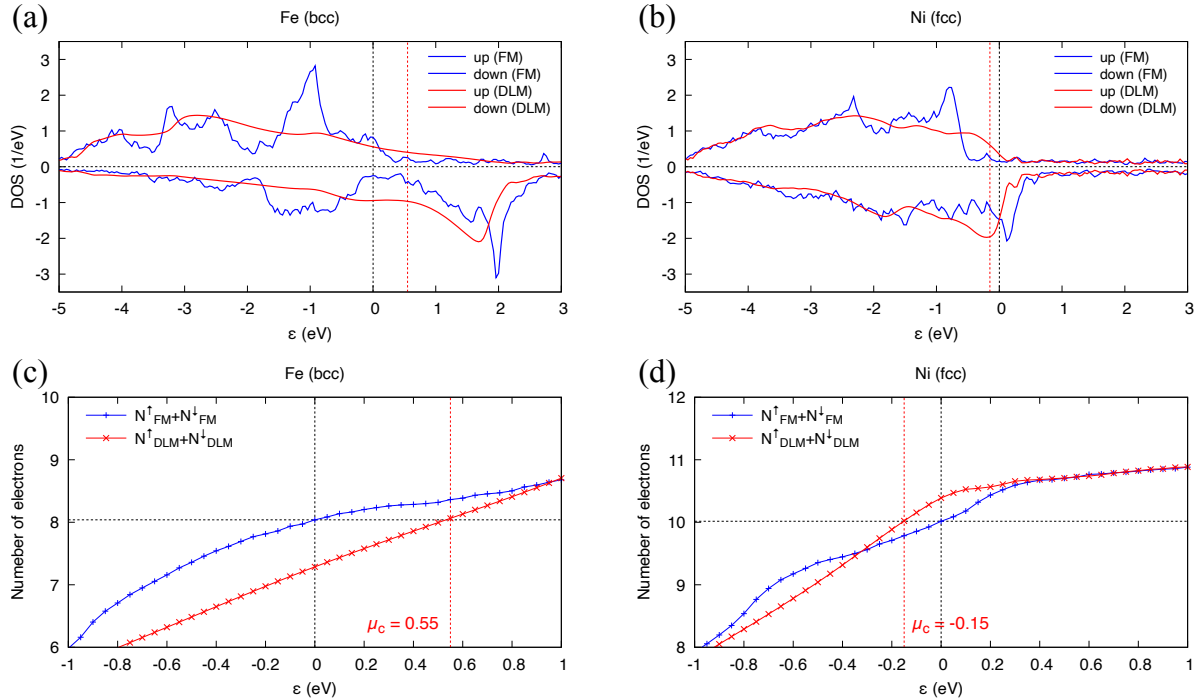


FIG. 4. Density of states (DOS) for the spin-up and spin-down components (panels (a) and (b)) and the integrated DOS (panels (c) and (d)). Panels (a) and (c) are the results for bcc Fe, while panels (b) and (d) are those for fcc Ni. In panels (a) and (b), blue lines represent the DOS for the ferromagnetic (FM) state, and red lines for the disordered local moment (DLM) state. The spin-up and spin-down components of both the FM and DLM states are plotted on the positive and negative sides, respectively. In panels (c) and (d), the vertical black lines indicate the chemical potential of the FM state ( $\mu = 0$ ), and the vertical red lines indicate the chemical potential  $\mu_c$  for the DLM state. The horizontal line indicates the number of electrons at  $\mu = 0$  in the *ab initio* tight-binding Hamiltonian.

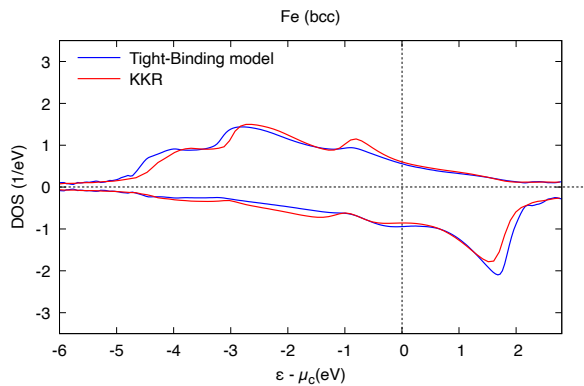


FIG. 5. Density of states of the DLM states obtained by the *ab initio* tight-binding method (blue) and the KKR method (red). The energy axis is calibrated by subtracting  $\mu_c$  from each result.

In contrast, approaches without an ordered reference state are better suited for exploring arbitrary magnetic configurations, e.g., when constructing a phase diagram of the system.

The approaches based on the fitting of the spin-configuration dependence of the total energy can also yield different results [81, 82]. In Ref. [81], they fit the spin Hamiltonian to the *ab initio* energies for a number of spin

spiral states with random wave vectors. Though they confine the spin Hamiltonian up to the biquadratic interaction and a four-spin interaction, they do not prioritize interactions between specific pairs during the fitting. On the other hand, in Ref. [82], while considering arbitrary spin interactions in the spin cluster expansion, they estimate the nearest-neighbor biquadratic interaction after the nearest-neighbor bilinear interaction. These different approaches could lead to the difference in the sign of the calculated biquadratic interactions. Additionally, as illustrated in Figs. 7 (a)-(f), the chemical potential dependence of the spin interactions could introduce ambiguity in theoretical results. Our approach is similar to the approach employed in Ref. [81] regarding the accessibility to various spin configurations, and our results are consistent with their result.

Although the individual spin interactions may vary due to the different choice of the reference state (i.e., the FM or DLM state), it is desirable that the macroscopic properties in the spin models do not depend on the reference states. Here, we compute the spin-wave dispersion in the long-wavelength region calculated by the FM-based method and SCE-DLM method. By extending LKAG to higher-order terms, the biquadratic interaction can be calculated for the TB model using

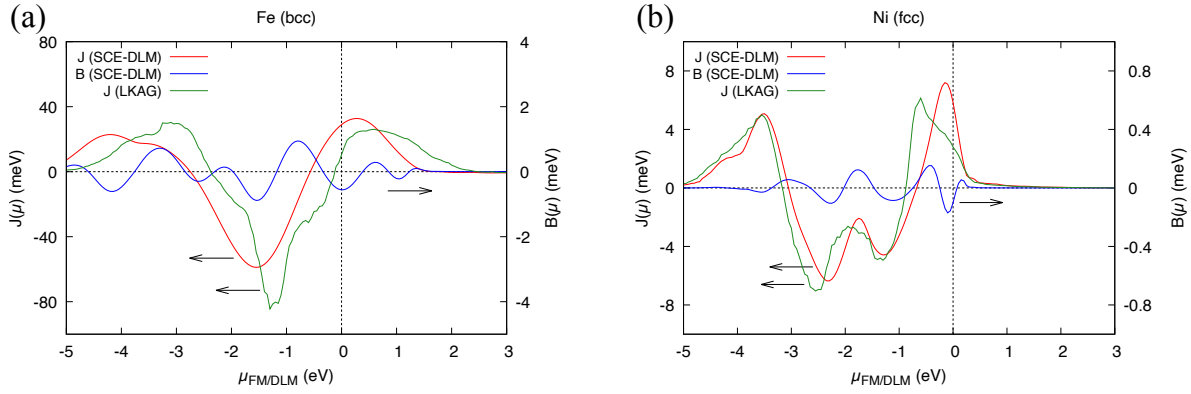


FIG. 6. Chemical potential dependence of the bilinear ( $J$ ) and biquadratic ( $B$ ) interactions for bcc Fe (a) and fcc Ni (b). Red, blue, and green lines indicate  $J$  and  $B$  calculated by SCE-DLM and  $J$  calculated by LKAG, respectively. Refer to the left vertical axis for  $J$ , and to the right vertical axis for  $B$ .

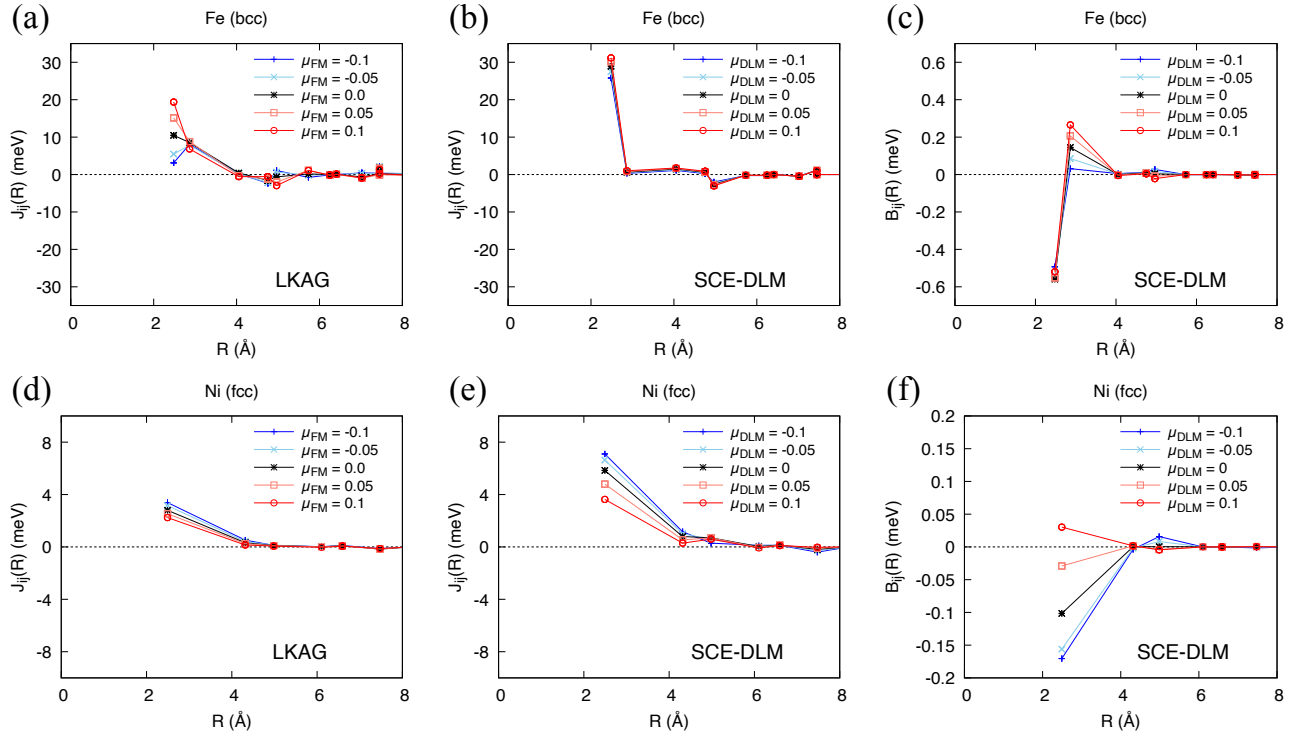


FIG. 7. The distance dependence of the bilinear ( $J_{ij}$ ) and the biquadratic ( $B_{ij}$ ) interactions. Panels (a)-(c) are the results for bcc Fe, and (d)-(f) are for fcc Ni.  $J_{ij}$  calculated by LKAG are shown in panels (a) and (d).  $J_{ij}(B_{ij})$  calculated by SCE-DLM are shown in panels (b) and (e) (c) and (f)). We also plot the values when we change  $\mu$ .

the following equations [39].

$$B_{ij} = \frac{1}{2\pi} \text{Im} \int d\epsilon f(\epsilon) \text{Tr} [\Delta V_i G_{ij} \Delta V_j G_{ji} \Delta V_i G_{ij} \Delta V_j G_{ji}] \quad (34)$$

$$[\Delta V_i]_{\ell\sigma, m\sigma'} = v_{\ell m}^i \sigma_{\sigma\sigma'}^x \quad (35)$$

where  $G_{ij}$  refers to the Green's function of the FM state with the polarization along the  $\hat{z}$ -axis, and  $\Delta V_i$  to the perturbation due to the infinitesimal spin rotation around the  $\hat{y}$ -axis,

respectively. In Fig. 9, we show the experimental spin-wave dispersion [87], and the theoretical ones calculated with  $J_{ij}$  and  $B_{ij}$  obtained from each method. The dispersion  $E(\mathbf{q})$  is computed via:

$$E(\mathbf{q}) = \sum_{j \neq i} [J_{ij}(1 - e^{i\mathbf{q} \cdot \mathbf{r}_{ij}}) + B_{ij}(1 - e^{2i\mathbf{q} \cdot \mathbf{r}_{ij}})] \quad (36)$$

In the FM-based method, the spin stiffness constant  $A$  (defined as  $E(\mathbf{q}) = A|\mathbf{q}|^2$ ) of the spin-wave dispersion calculated from  $J_{ij}$  alone is underestimated compared to the ex-

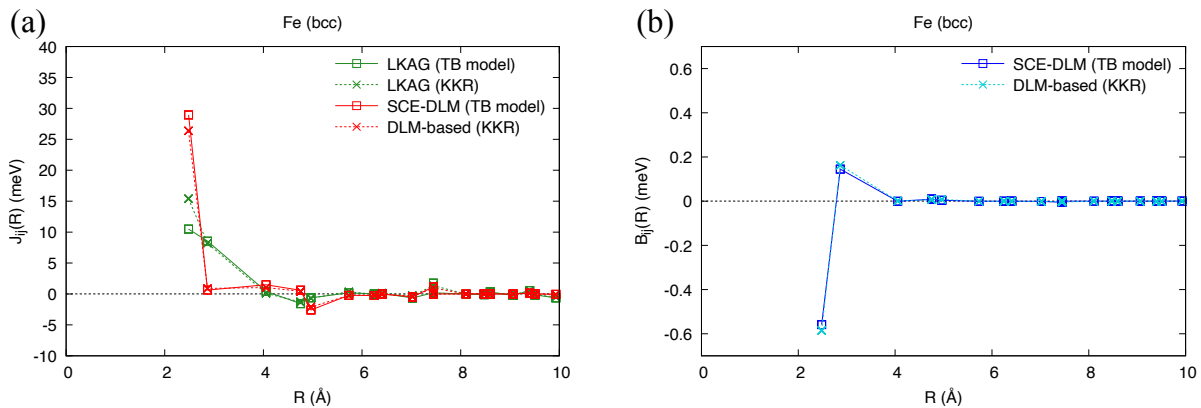


FIG. 8. Bilinear (a) and biquadratic (b) interactions of bcc Fe as a function of the distance ( $R$ ) between the  $i$ -th and  $j$ -th site. The green (red and blue) lines are those calculated using LKAG (SCE-DLM) at  $\mu_{\text{FM(DLM)}} = 0$ . Among the same color lines, solid (dotted) lines are the results of the *ab initio* tight-binding (KKR) method.

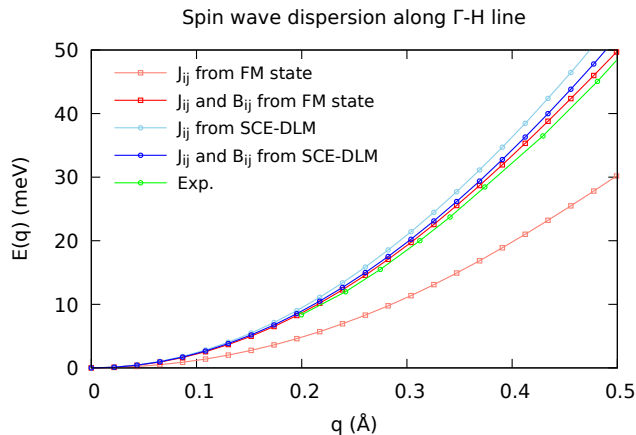


FIG. 9. Spin-wave dispersion of bcc Fe along the  $\Gamma$ -H line. The green curve is the experimental values at room temperature [87]. The light-red (red) curve is the dispersion calculated from the bilinear interactions only (and the biquadratic interactions) using the FM-based method [39]. The light-blue and blue curves are those calculated using SCE-DLM.

perimental value. However,  $B_{ij}$  is calculated to be positive and brings  $A$  closer to the experimental value. On the other hand, for the SCE-DLM method,  $A$  is slightly overestimated when calculated from  $J_{ij}$  alone. Then,  $B_{ij}$ , having a smaller value than the one computed via the FM-based method, is negative and brings  $A$  closer to the experimental value. Namely, by adding  $B_{ij}$  to  $J_{ij}$ , the spin-wave dispersion aligns well with the experimental result in both SCE-DLM and LKAG approaches.

## VI. CONCLUSION

We developed an SCE-DLM approach for *ab initio* tight-binding Hamiltonians by combining the spin cluster expan-

sion and the disordered local moment (DLM) approach, which was originally available only with the Green's function methods, such as the KKR method. We first applied the SCE-DLM scheme to the one-dimensional two-orbital Hubbard model and found that the calculated biquadratic interactions closely aligned with those for the effective quantum spin model in the strongly correlated limit (super-exchange). This alignment suggests the broad applicability of the SCE-DLM approach to a wide variety of strongly correlated compounds with large local magnetic moments. We subsequently applied this scheme to two prototypical magnets, bcc Fe and fcc Ni. Our results are consistent with previous theoretical investigations [39, 81], confirming the reliability of the presented method. In addition, we corroborated our *ab initio* tight-binding approach by comparing our results with those obtained via the KKR multiple scattering theory and showing a good quantitative agreement between these two distinct methods.

The SCE-DLM scheme for the *ab initio* tight-binding Hamiltonian has the advantage of not inducing a reference state dependence of the magnetic interactions and requiring only tight-binding parameters which can be computed based on different *ab initio* schemes such as plane-wave basis and pseudo-atomic localized basis functions [88, 89]. The extension of our method to incorporate relativistic chiral (Dzyaloshinskii-Moriya like) and multi-spin / multi-site interactions offers a promising approach to systematically compute the magnetic interactions between local moments to arbitrary order. It will be a convenient tool for understanding and predicting nontrivial exotic magnetic phases induced by higher-order and relativistic spin interactions in an *ab initio* framework.

## ACKNOWLEDGEMENTS

We would like to thank Katsuhiro Tanaka and Hiroshi Katsumoto for fruitful discussions. This work was supported by RIKEN Junior Research Associate Program. This work was supported by the RIKEN TRIP initiative (RIKEN

Quantum, Advanced General Intelligence for Science Program, Multi-Electron Group). We acknowledge the financial support by Grant-in-Aids for Scientific Research (JSPS KAKENHI) Grant Numbers JP21H04437, JP21H04990, JP19H05825, JP22H00290, and JP24K00581, JST-CREST No. JPMJCR18T3, No. JPMJCR23O4, JST-ASPIRE No. JPMJAP2317, JST-Mirai No. JPMJMI20A1. T. N. was supported by JST, PRESTO Grant Number JPMJPR20L7, Japan. J. B. was supported by the Alexander von Humboldt Foundation through the Feodor Lynen Research Fellowship for Post-docs.

### Appendix A: Asymptotic form for single-orbital tight-binding model

In Section IV A, a tight-binding Hamiltonian with a spin splitting was derived from the two-orbital Hubbard Hamiltonian. Here, let us look into a simpler case, i.e., a one-dimensional single-orbital model with the mean-field approximation:

$$\mathcal{H} = - \sum_{\langle i,j \rangle, \sigma} (t c_{i\sigma}^\dagger c_{j\sigma} + \text{h.c.}) - B\sigma_z. \quad (\text{A1})$$

We can analytically obtain the on-site component of the Green's function of the DLM state for this model as follows:

$$\bar{G}_{ii}(\epsilon) = \left\{ \text{sgn}(\text{Re}(\epsilon - \tilde{\Sigma}^i)) \sqrt{(\epsilon - \tilde{\Sigma}^i)^2 - 4t^2} \right\}^{-1}. \quad (\text{A2})$$

By substituting this expression of  $\bar{G}_{ii}$  to Eqs. (15) and (16) with  $V(\pm\hat{z}) = \mp B$  for the up and down spins, the CPA condition yields the equation for the self-energy  $\Sigma$  as follows:

$$0 = 2\epsilon\tilde{\Sigma}^3 - (2B^2 - 4t^2 + \epsilon^2)\tilde{\Sigma}^2 + B^4 \quad (\text{A3})$$

Let us now consider deriving the asymptotic expression of the exchange interaction for the limit of strong and weak correlation based on SCE-DLM. Starting with Eq. (21), we expand it as follows:

$$\begin{aligned} J_{ij}^{LL'} &\sim \frac{1}{\pi} \text{Im} \int d\epsilon f(\epsilon) \iint d^2\mathbf{e}_i d^2\mathbf{e}_j Y_L(\mathbf{e}_i) Y_{L'}(\mathbf{e}_j) \\ &\times \left[ T_i(\mathbf{e}_i) \bar{G}_{ij} T_j(\mathbf{e}_j) \bar{G}_{ji} + \right. \\ &\left. \frac{1}{2} T_i(\mathbf{e}_i) \bar{G}_{ij} T_j(\mathbf{e}_j) \bar{G}_{ji} T_i(\mathbf{e}_i) \bar{G}_{ij} T_j(\mathbf{e}_j) \bar{G}_{ji} \right], \end{aligned} \quad (\text{A4})$$

Here, we utilize the Taylor expansion,  $\log(1-x) \sim -x - x^2/2$ . Though there are other higher-order terms in the expansion, these terms are sufficient to obtain leading-order terms of the bilinear and biquadratic interactions in the strong and itinerant limits. We also derive the expression of the scattering operator  $T_i(\mathbf{e}_i)$  by applying the CPA condition in Eq.(A3) and introducing the inverse of the Green's function as  $A = 1/\bar{G}_{ii}(\epsilon)$ ,

$$T_i(\mathbf{e}_i) = - \frac{BA^2}{(A + \tilde{\Sigma})^2 - B^2} \begin{pmatrix} \cos\theta & e^{-i\phi} \sin\theta \\ e^{i\phi} \sin\theta & -\cos\theta \end{pmatrix}. \quad (\text{A5})$$

### 1. Itinerant limit

In the limit of  $B \ll t$ , the CPA condition becomes  $0 = 2\epsilon\tilde{\Sigma}^3 + (4t^2 - \epsilon^2)\tilde{\Sigma}^2$  and the solutions of this equation are:

$$\tilde{\Sigma}(\epsilon) = 0, \quad \frac{\epsilon}{2} + \frac{2t^2}{\epsilon} \quad (\text{A6})$$

As the latter solution is unphysical in the limit of  $\epsilon \rightarrow \pm\infty$ , the solution of the CPA condition approaches  $\tilde{\Sigma}(\epsilon) \rightarrow 0$ . By substituting this self-energy solution to Eq. (A5), the scattering operator becomes

$$T_i(\mathbf{e}_i) \rightarrow -B \begin{pmatrix} \cos\theta & e^{-i\phi} \sin\theta \\ e^{i\phi} \sin\theta & -\cos\theta \end{pmatrix}. \quad (\text{A7})$$

We here use that  $A \rightarrow \sqrt{\epsilon^2 - 4t^2}$ . The first term of the right-hand side in Eq. (A4) remains finite only for  $l = 1$ . This corresponds to the fact that higher-order interactions ( $l \geq 2$ ) require perturbations higher than the second order. It is also important to note again that  $J_{ij}^{(l,m)(l,m)}$  depends solely on  $l$  and is independent of  $m$  in the absence of SOC. Then, we can easily show that the bilinear interaction in SCE-DLM (Eq. (A4)) becomes equivalent to that of LKAG in this limit, hence yielding the RKKY interaction [90–92] as follows:

$$\begin{aligned} J_{ij} &= \frac{3}{8\pi} J_{ij}^{(1,0)(1,0)} \\ &\rightarrow \frac{B^2}{\pi N^2} \sum_{k,q} \text{Im} \int d\epsilon f(\epsilon) G_{k+q}^0 G_k^0 e^{iqR_{ij}} \\ &= \frac{B^2}{\pi N} \sum_q \chi(q) e^{iqR_{ij}}, \end{aligned} \quad (\text{A8})$$

where  $N, G_k^0 = (\epsilon - \epsilon_k + i\delta)^{-1}, \chi(q)$  is the number of sites, the retarded Green's function, and the spin susceptibility of non-interacting electrons, respectively. Here we use an infinitesimally small value  $\delta$ , and  $\chi(q)$  is defined as follows:

$$\chi(q) = \frac{1}{\pi N} \sum_k \text{Im} \int d\epsilon f(\epsilon) G_{k+q}^0 G_k^0 \quad (\text{A9})$$

$$= \frac{1}{N} \sum_k \frac{f(\epsilon_k) - f(\epsilon_{k+q})}{\epsilon_{k+q} - \epsilon_k + i\delta}. \quad (\text{A10})$$

With SCE-DLM, we can obtain higher-order interactions such as the biquadratic interaction. Indeed, we can derive the biquadratic interaction by considering higher order terms in Eq. (A4). The asymptotic expression of the biquadratic interaction becomes:

$$\begin{aligned} B_{ij} &= \frac{15}{16\pi} J_{ij}^{(2,0)(2,0)} \\ &\rightarrow \frac{B^4}{\pi N^2} \sum_{k,q,k',q'} \text{Im} \int d\epsilon f(\epsilon) G_{k+q}^0 G_k^0 G_{k'+q'}^0 G_{k'}^0 e^{i(q+q')R_{ij}}. \end{aligned} \quad (\text{A11})$$

As discussed in Ref. [12], contributions from the  $k = k', q = q'$  case always yield a negative biquadratic interaction between any sites and cause instability of the collinear spin structures.

## 2. Strongly correlated limit

In the limit of strong correlation  $U \sim B \gg t$ , the CPA condition becomes to  $2\epsilon\tilde{\Sigma}^3 - (2B^2 + \epsilon^2)\tilde{\Sigma}^2 + B^4 = 0$  and the solutions are given as:

$$\tilde{\Sigma}(\epsilon) = \frac{B^2}{\epsilon}, \frac{\epsilon \pm \sqrt{\epsilon^2 + 8B^2}}{4}. \quad (\text{A12})$$

Similarly to the itinerant case, the solution of the self-energy is  $\tilde{\Sigma}(\epsilon) \rightarrow B^2/\epsilon$ .

We start from the DLM state without the hopping term  $t$ . The retarded Green's function for this non-perturbed state is provided as:

$$\overline{G}_{ii}^{(0)}(\epsilon) = \frac{\delta_{ij}}{\epsilon - \tilde{\Sigma} + i\delta}, \quad (\text{A13})$$

where the superscript (0) stands for the non-perturbed term. By treating the hopping term as the perturbation, we can derive the expression for the Green's function, considering terms up to the first order perturbation:

$$\begin{aligned} \overline{G}_{ij}^{(1)}(\epsilon) &= \frac{1}{\epsilon - \tilde{\Sigma} + i\delta} t \frac{1}{\epsilon - \tilde{\Sigma} + i\delta} \\ &= \frac{t}{(\epsilon - \tilde{\Sigma} + i\delta)^2}, \end{aligned} \quad (\text{A14})$$

where the superscript (1) stands for the first order perturbation term and  $j$  is the nearest-neighbor sites of site  $i$ .

Subsequently, we evaluate the scattering operator as follows:

$$T_i(\mathbf{e}_i) \rightarrow -\frac{(\epsilon - \tilde{\Sigma})^2}{\epsilon^2 - B^2} B \begin{pmatrix} \cos \theta & e^{-i\phi} \sin \theta \\ e^{i\phi} \sin \theta & -\cos \theta \end{pmatrix}, \quad (\text{A15})$$

where we use  $A \rightarrow \epsilon - \tilde{\Sigma}$  in this limit. By substituting Eqs. (A14) and (A15) into the first term of Eq. (A4), we obtain the following asymptotic expression for the  $l = 1$  interaction between nearest neighbor sites:

$$\begin{aligned} J_{ij}^{(1,m)(1,m)} &\sim -\frac{2}{\pi} \frac{4\pi}{3} \text{Im} \int^{\epsilon_F} d\epsilon \frac{t^2 B^2}{(\epsilon - \Sigma + i\delta)^4} \frac{(\epsilon - \Sigma)^4}{(\epsilon^2 - B^2)^2} \\ &= -\frac{4}{3i} \int_C dz \frac{t^2 B^2}{(z - B)^2 (z + B)^2}. \end{aligned} \quad (\text{A16})$$

We illustrate an integration contour in Eq. (A16) in Fig. 10.

We subsequently derive an asymptotic expression for the bilinear interaction.

$$J_{ij} = \frac{3}{8\pi} J_{ij}^{(1,0)(1,0)} \rightarrow -\frac{t^2}{4B} \sim -\frac{t^2}{2U} \quad (\text{A17})$$

We can obtain the expression for the biquadratic interaction by following the same process.

$$B_{ij} = \frac{15}{16\pi} J_{ij}^{(2,0)(2,0)} \rightarrow -\frac{5}{4} \frac{t^4}{U^3}. \quad (\text{A18})$$

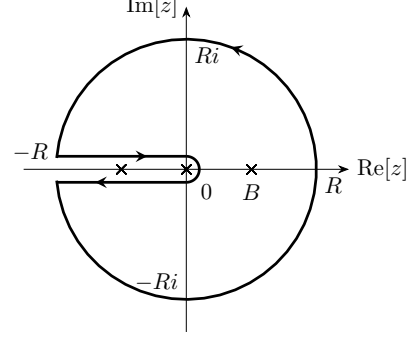


FIG. 10. Integration contour of Eq. (A16). We take the  $R \rightarrow \infty$  limit in the integration.

These asymptotic expressions for the bilinear and biquadratic interactions are equivalent to those obtained by the conventional LKAG method and its extensions[39] in both the strongly correlated and the itinerant limits. However, it is crucial to recognize that the initial magnetic state in SCE-DLM, the DLM state, differs from the ferromagnetic state used in these methods. Furthermore, it is noteworthy that when using SCE-DLM and the method described in Ref. [39], the biquadratic interaction remains finite even in a single-orbital system, in contrast to the effective quantum spin model where this term inevitably vanishes. In the quantum spin model of a  $S = 1/2$  system, this term corresponding to a fourth-order perturbation is merely a correction to the bilinear interaction. However, the classical treatment of spins in electron systems ensures that these higher-order interactions remain finite even in a single-orbital system. Therefore, it is not appropriate to simply compare this expression with Eq. (28).

- 
- [1] T. Jungwirth, X. Marti, P. Wadley, and J. Wunderlich, Antiferromagnetic spintronics, *Nature Nanotechnology* **11**, 231 (2016).
  - [2] V. Baltz, A. Manchon, M. Tsoi, T. Moriyama, T. Ono, and Y. Tserkovnyak, Antiferromagnetic spintronics, *Rev. Mod. Phys.* **90**, 015005 (2018).
  - [3] T. Jungwirth, J. Sinova, A. Manchon, X. Marti, J. Wunderlich, and C. Felser, The multiple directions of antiferromagnetic spintronics, *Nature Physics* **14**, 200 (2018).
  - [4] W. Heisenberg, Mehrkörperproblem und resonanz in der quan-

- tenmechanik, *Zeitschrift für Physik* **38**, 411 (1926).
- [5] I. Dzyaloshinsky, A thermodynamic theory of "weak" ferromagnetism of antiferromagnetics, *Journal of Physics and Chemistry of Solids* **4**, 241 (1958).
- [6] T. Moriya, Anisotropic superexchange interaction and weak ferromagnetism, *Phys. Rev.* **120**, 91 (1960).
- [7] A. Bogdanov and D. Yablonski, Thermodynamically stable "vortices" in magnetically ordered crystals. The mixed state of magnets, *Zh. Eksp. Teor. Fiz.* **95**, 178 (1989).

- [8] N. Nagaosa and Y. Tokura, Topological properties and dynamics of magnetic skyrmions, *Nature nanotechnology* **8**, 899 (2013).
- [9] S. Hayami and Y. Motome, Topological spin crystals by itinerant frustration, *Journal of Physics: Condensed Matter* **33**, 443001 (2021).
- [10] E. Simon, A. Donges, L. Szunyogh, and U. Nowak, Non-collinear antiferromagnetic states in ru-based heusler compounds induced by biquadratic coupling, *Phys. Rev. Mater.* **4**, 084408 (2020).
- [11] R. N. Bhatt and K. Yang, Non-Heisenberg couplings and ferromagnetic instability in a random antiferromagnetic spin-1 chain, *Journal of Applied Physics* **83**, 7231 (1998), [https://pubs.aip.org/aip/jap/article-pdf/83/11/7231/19267600/7231\\_1\\_online.pdf](https://pubs.aip.org/aip/jap/article-pdf/83/11/7231/19267600/7231_1_online.pdf).
- [12] S. Hayami, R. Ozawa, and Y. Motome, Effective bilinear-biquadratic model for noncoplanar ordering in itinerant magnets, *Phys. Rev. B Condens. Matter* **95**, 224424 (2017).
- [13] S. Okumura, S. Hayami, Y. Kato, and Y. Motome, Magnetic hedgehog lattice in a centrosymmetric cubic metal, *Journal of the Physical Society of Japan* **91**, 093702 (2022), <https://doi.org/10.7566/JPSJ.91.093702>.
- [14] S. Seo, S. Hayami, Y. Su, S. M. Thomas, F. Ronning, E. D. Bauer, J. D. Thompson, S.-Z. Lin, and P. F. S. Rosa, Spin-texture-driven electrical transport in multi-q antiferromagnets, *Communications Physics* **4**, 58 (2021).
- [15] B. G. Ueland, C. F. Miclea, Y. Kato, O. Ayala-Valenzuela, R. D. McDonald, R. Okazaki, P. H. Tobash, M. A. Torrez, F. Ronning, R. Movshovich, Z. Fisk, E. D. Bauer, I. Martin, and J. D. Thompson, Controllable chirality-induced geometrical hall effect in a frustrated highly correlated metal, *Nature Communications* **3**, 1067 (2012).
- [16] J. A. M. Paddison, H. Zhang, J. Yan, M. J. Cliffe, S.-H. Do, S. Gao, M. B. Stone, D. Dahlbom, K. Barros, C. D. Batista, and A. D. Christianson, Cubic double perovskites host noncoplanar spin textures (2023), [arXiv:2301.11395 \[cond-mat.str-el\]](https://arxiv.org/abs/2301.11395).
- [17] H. Takagi, R. Takagi, S. Minami, T. Nomoto, K. Ohishi, M. T. Suzuki, Y. Yanagi, M. Hirayama, N. D. Khanh, K. Karube, H. Saito, D. Hashizume, R. Kiyonagi, Y. Tokura, R. Arita, T. Nakajima, and S. Seki, Spontaneous topological hall effect induced by non-coplanar antiferromagnetic order in intercalated van der waals materials, *Nature Physics* **19**, 961 (2023).
- [18] P. Park, W. Cho, C. Kim, Y. An, Y.-G. Kang, M. Avdeev, R. Sibille, K. Iida, R. Kajimoto, K. H. Lee, W. Ju, E.-J. Cho, H.-J. Noh, M. J. Han, S.-S. Zhang, C. D. Batista, and J.-G. Park, Tetrahedral triple-q magnetic ordering and large spontaneous hall conductivity in the metallic triangular antiferromagnet  $\text{Co}_1/3\text{Ta}_2$ , *Nature Communications* **14**, 8346 (2023).
- [19] A. Szilva, Y. Kvashnin, E. A. Stepanov, L. Nordström, O. Eriksson, A. I. Lichtenstein, and M. I. Katsnelson, Quantitative theory of magnetic interactions in solids, *Rev. Mod. Phys.* **95**, 035004 (2023).
- [20] T. Oguchi, K. Terakura, and N. Hamada, Magnetism of iron above the curie temperature, *Journal of Physics F: Metal Physics* **13**, 145 (1983).
- [21] A. I. Lichtenstein, M. I. Katsnelson, and V. A. Gubanov, Exchange interactions and spin-wave stiffness in ferromagnetic metals, *Journal of Physics F: Metal Physics* **14**, L125 (1984).
- [22] T. Nomoto, T. Koretsune, and R. Arita, Local force method for the ab initio tight-binding model: Effect of spin-dependent hopping on exchange interactions, *Phys. Rev. B* **102**, 014444 (2020).
- [23] A. Sakuma, First principles study on the exchange constants of the 3d transition metals, *Journal of the Physical Society of Japan* **68**, 620 (1999), <https://doi.org/10.1143/JPSJ.68.620>.
- [24] A. Sakuma, First-principles study on the non-collinear magnetic structures of disordered alloys, *Journal of the Physical Society of Japan* **69**, 3072 (2000), <https://doi.org/10.1143/JPSJ.69.3072>.
- [25] Y. Nomura, T. Nomoto, M. Hirayama, and R. Arita, Magnetic exchange coupling in cuprate-analog  $d^9$  nickelates, *Phys. Rev. Res.* **2**, 043144 (2020).
- [26] T. Nomoto, T. Koretsune, and R. Arita, Formation mechanism of the helical  $q$  structure in gd-based skyrmion materials, *Phys. Rev. Lett.* **125**, 117204 (2020).
- [27] T. Hatanaka, T. Nomoto, and R. Arita, Magnetic interactions in intercalated transition metal dichalcogenides: A study based on *ab initio* model construction, *Phys. Rev. B* **107**, 184429 (2023).
- [28] J. Bouaziz, E. Menvide-Tapia, S. Blügel, and J. B. Staunton, Fermi-surface origin of skyrmion lattices in centrosymmetric rare-earth intermetallics, *Phys. Rev. Lett.* **128**, 157206 (2022).
- [29] J. Bouaziz, G. Bihlmayer, C. E. Patrick, J. B. Staunton, and S. Blügel, Origin of incommensurate magnetic order in the  $r\text{AlSi}$  magnetic weyl semimetals ( $r = \text{Pr, Nd, Sm}$ ), *Phys. Rev. B* **109**, L201108 (2024).
- [30] H. Miao, J. Bouaziz, G. Fabbris, W. R. Meier, F. Z. Yang, H. X. Li, C. Nelson, E. Vescovo, S. Zhang, A. D. Christianson, H. N. Lee, Y. Zhang, C. D. Batista, and S. Blügel, Spontaneous chirality flipping in an orthogonal spin-charge ordered topological magnet, *Phys. Rev. X* **14**, 011053 (2024).
- [31] R. Logemann, A. N. Rudenko, M. I. Katsnelson, and A. Kirilyuk, Exchange interactions in transition metal oxides: the role of oxygen spin polarization, *Journal of Physics: Condensed Matter* **29**, 335801 (2017).
- [32] L. Udvardi, L. Szunyogh, K. Palotás, and P. Weinberger, First-principles relativistic study of spin waves in thin magnetic films, *Phys. Rev. B* **68**, 104436 (2003).
- [33] H. Ebert and S. Mankovsky, Anisotropic exchange coupling in diluted magnetic semiconductors: Ab initio spin-density functional theory, *Phys. Rev. B* **79**, 045209 (2009).
- [34] I. V. Solov'ev and K. Terakura, Zone boundary softening of the Spin-Wave dispersion in doped ferromagnetic manganites, *Phys. Rev. Lett.* **82**, 2959 (1999).
- [35] S. Lounis and P. H. Dederichs, Mapping the magnetic exchange interactions from first principles: Anisotropy anomaly and application to fe, ni, and co, *Phys. Rev. B* **82**, 180404 (2010).
- [36] A. Szilva, M. Costa, A. Bergman, L. Szunyogh, L. Nordström, and O. Eriksson, Interatomic exchange interactions for finite-temperature magnetism and nonequilibrium spin dynamics, *Phys. Rev. Lett.* **111**, 127204 (2013).
- [37] M. dos Santos Dias, S. Brinker, A. Lászlóffy, B. Nyári, S. Blügel, L. Szunyogh, and S. Lounis, Proper and improper chiral magnetic interactions, *Phys. Rev. B* **103**, L140408 (2021).
- [38] A. Szilva, M. Costa, A. Bergman, L. Szunyogh, L. Nordström, and O. Eriksson, Interatomic exchange interactions for finite-temperature magnetism and nonequilibrium spin dynamics, *Phys. Rev. Lett.* **111**, 127204 (2013).
- [39] S. Mankovsky, S. Polesya, and H. Ebert, Extension of the standard heisenberg hamiltonian to multispin exchange interactions, *Phys. Rev. B* **101**, 174401 (2020).
- [40] P. Kurz, G. Bihlmayer, K. Hirai, and S. Blügel, Three-dimensional spin structure on a two-dimensional lattice: Mn/cu(111), *Phys. Rev. Lett.* **86**, 1106 (2001).
- [41] S. Grytsiuk, J.-P. Hanke, M. Hoffmann, J. Bouaziz, O. Gomonay, G. Bihlmayer, S. Lounis, Y. Mokrousov, and S. Blügel, Topological-chiral magnetic interactions driven by

- emergent orbital magnetism, *Nature communications* **11**, 511 (2020).
- [42] B. Ujfalussy, X.-D. Wang, D. Nicholson, W. Shelton, G. Stocks, Y. Wang, and B. Györffy, Constrained density functional theory for first principles spin dynamics, *Journal of applied physics* **85**, 4824 (1999).
- [43] A. J. Pindor, J. Staunton, G. M. Stocks, and H. Winter, Disordered local moment state of magnetic transition metals: a self-consistent kkr cpa calculation, *Journal of Physics F: Metal Physics* **13**, 979 (1983).
- [44] J. B. Staunton, L. Szunyogh, A. Buruzs, B. L. Györffy, S. Osttanin, and L. Udvardi, Temperature dependence of magnetic anisotropy: An ab initio approach, *Phys. Rev. B* **74**, 144411 (2006).
- [45] C. E. Patrick and J. B. Staunton, Rare-earth/transition-metal magnets at finite temperature: Self-interaction-corrected relativistic density functional theory in the disordered local moment picture, *Phys. Rev. B* **97**, 224415 (2018).
- [46] J. Bouaziz, C. E. Patrick, and J. B. Staunton, Crucial role of fe in determining the hard magnetic properties of  $\text{Nd}_2\text{Fe}_{14}\text{B}$ , *Phys. Rev. B* **107**, L020401 (2023).
- [47] R. Drautz and M. Fähnle, Spin-cluster expansion: Parametrization of the general adiabatic magnetic energy surface with ab initio accuracy, *Phys. Rev. B* **69**, 104404 (2004).
- [48] R. Drautz and M. Fähnle, Parametrization of the magnetic energy at the atomic level, *Phys. Rev. B* **72**, 212405 (2005).
- [49] L. Szunyogh, L. Udvardi, J. Jackson, U. Nowak, and R. Chantrell, Atomistic spin model based on a spin-cluster expansion technique: Application to the  $\text{IrMn}_3/\text{Co}$  interface, *Phys. Rev. B* **83**, 024401 (2011).
- [50] E. Simon, R. Yanes, S. Khmelevskiy, K. Palotás, L. Szunyogh, and U. Nowak, Magnetism and exchange-bias effect at the  $\text{Mn}/\text{Fe}$  interface, *Phys. Rev. B* **98**, 094415 (2018).
- [51] B. Nyári, A. Deák, and L. Szunyogh, Weak ferromagnetism in hexagonal  $\text{Mn}_3\text{Z}$  alloys ( $\text{Z} = \text{Sn}, \text{Ge}, \text{Ga}$ ), *Phys. Rev. B* **100**, 144412 (2019).
- [52] E. Simon, A. Donges, L. Szunyogh, and U. Nowak, Non-collinear antiferromagnetic states in Ru-based Heusler compounds induced by biquadratic coupling, *Phys. Rev. Mater.* **4**, 084408 (2020).
- [53] T. Dannegger, A. Deák, L. Rózsa, E. Galindez-Ruales, S. Das, E. Baek, M. Kläui, L. Szunyogh, and U. Nowak, Magnetic properties of hematite revealed by an ab initio parameterized spin model, *Phys. Rev. B* **107**, 184426 (2023).
- [54] A. Deák, L. Szunyogh, and B. Ujfalussy, Thickness-dependent magnetic structure of ultrathin  $\text{Fe}/\text{Ir}(001)$  films: From spin-spiral states toward ferromagnetic order, *Phys. Rev. B Condens. Matter* **84**, 224413 (2011).
- [55] J. B. Staunton, R. Banerjee, M. d. S. Dias, A. Deak, and L. Szunyogh, Fluctuating local moments, itinerant electrons, and the magnetocaloric effect: Compositional hypersensitivity of  $\text{FeRh}$ , *Phys. Rev. B* **89**, 054427 (2014).
- [56] R. Zeller, Recent advances in the Korringa-Kohn-Rostoker Green function method, in *EPJ Web of Conferences*, Vol. 78 (EDP Sciences, 2014) p. 05002.
- [57] X. Qin, J. Chen, Z. Luo, L. Wan, J. Li, S. Jiao, Z. Zhang, Q. Jiang, W. Hu, H. An, and J. Yang, High performance computing for first-principles Kohn-Sham density functional theory towards exascale supercomputers, *CCF Transactions on High Performance Computing* **5**, 26 (2023).
- [58] P. Soven, Coherent-potential model of substitutional disordered alloys, *Phys. Rev.* **156**, 809 (1967).
- [59] N. Ito, T. Nomoto, K. Kobayashi, S. Mankovsky, K. Nomura, R. Arita, H. Ebert, and T. Koretsune, Wannier-based implementation of the coherent potential approximation with applications to Fe-based transition metal alloys, *Phys. Rev. B* **105**, 125136 (2022).
- [60] P. Lloyd, Wave propagation through an assembly of spheres: Ii. the density of single-particle eigenstates, *Proceedings of the Physical Society* **90**, 207 (1967).
- [61] R. Zeller, Lloyd's formula in multiple-scattering calculations with finite temperature, *Journal of Physics: Condensed Matter* **17**, 5367 (2005).
- [62] V. Lebedev, Quadratures on a sphere, *USSR Computational Mathematics and Mathematical Physics* **16**, 10 (1976).
- [63] H. Shinaoka, J. Otsuki, M. Ohzeki, and K. Yoshimi, Compressing Green's function using intermediate representation between imaginary-time and real-frequency domains, *Phys. Rev. B* **96**, 035147 (2017).
- [64] N. Chikano, K. Yoshimi, J. Otsuki, and H. Shinaoka, ir-basis: Open-source database and software for intermediate-representation basis functions of imaginary-time Green's function, *Computer Physics Communications* **240**, 181 (2019).
- [65] P. Giannozzi, S. Baroni, N. Bonini, M. Calandra, R. Car, C. Cavazzoni, D. Ceresoli, G. L. Chiarotti, M. Cococcioni, I. Dabo, A. D. Corso, S. de Gironcoli, S. Fabris, G. Fratesi, R. Gebauer, U. Gerstmann, C. Gougoussis, A. Kokalj, M. Lazzeri, L. Martin-Samos, N. Marzari, F. Mauri, R. Mazzarello, S. Paolini, A. Pasquarello, L. Paulatto, C. Sbraccia, S. Scandolo, G. Sclauzero, A. P. Seitsonen, A. Smogunov, P. Umari, and R. M. Wentzcovitch, Quantum espresso: a modular and open-source software project for quantum simulations of materials, *Journal of Physics: Condensed Matter* **21**, 395502 (2009).
- [66] P. Giannozzi, O. Andreussi, T. Brumme, O. Bunau, M. B. Nardelli, M. Calandra, R. Car, C. Cavazzoni, D. Ceresoli, M. Cococcioni, N. Colonna, I. Carnimeo, A. D. Corso, S. de Gironcoli, P. Delugas, R. A. DiStasio, A. Ferretti, A. Floris, G. Fratesi, G. Fugallo, R. Gebauer, U. Gerstmann, F. Giustino, T. Gorni, J. Jia, M. Kawamura, H.-Y. Ko, A. Kokalj, E. Küçükbenli, M. Lazzeri, M. Marsili, N. Marzari, F. Mauri, N. L. Nguyen, H.-V. Nguyen, A. O. de-la Roza, L. Paulatto, S. Poncé, D. Rocca, R. Sabatini, B. Santra, M. Schlipf, A. P. Seitsonen, A. Smogunov, I. Timrov, T. Thonhauser, P. Umari, N. Vast, X. Wu, and S. Baroni, Advanced capabilities for materials modelling with quantum espresso, *Journal of Physics: Condensed Matter* **29**, 465901 (2017).
- [67] A. Dal Corso, Pseudopotentials periodic table: From h to pu, *Computational Materials Science* **95**, 337 (2014).
- [68] P. E. Blöchl, Projector augmented-wave method, *Phys. Rev. B* **50**, 17953 (1994).
- [69] G. Kresse and D. Joubert, From ultrasoft pseudopotentials to the projector augmented-wave method, *Phys. Rev. B* **59**, 1758 (1999).
- [70] J. P. Perdew, K. Burke, and M. Ernzerhof, Generalized gradient approximation made simple, *Phys. Rev. Lett.* **77**, 3865 (1996).
- [71] N. Marzari and D. Vanderbilt, Maximally localized generalized Wannier functions for composite energy bands, *Phys. Rev. B* **56**, 12847 (1997).
- [72] I. Souza, N. Marzari, and D. Vanderbilt, Maximally localized Wannier functions for entangled energy bands, *Phys. Rev. B* **65**, 035109 (2001).
- [73] A. A. Mostofi, J. R. Yates, Y.-S. Lee, I. Souza, D. Vanderbilt, and N. Marzari, Wannier90: A tool for obtaining maximally-localised Wannier functions, *Computer Physics Communications* **178**, 685 (2008).
- [74] G. Pizzi, V. Vitale, R. Arita, S. Blügel, F. Freimuth, G. Géranton, M. Gibertini, D. Gresch, C. Johnson, T. Koret-

- sune, J. Ibañez-Azpiroz, H. Lee, J.-M. Lihm, D. Marchand, A. Marrazzo, Y. Mokrousov, J. I. Mustafa, Y. Nohara, Y. Nomura, L. Paulatto, S. Poncé, T. Ponweiser, J. Qiao, F. Thöle, S. S. Tsirkin, M. Wierzbowska, N. Marzari, D. Vanderbilt, I. Souza, A. A. Mostofi, and J. R. Yates, Wannier90 as a community code: new features and applications, *Journal of Physics: Condensed Matter* **32**, 165902 (2020).
- [75] P. Rössmann, D. Antognini Silva, G. Géranton, D. S. G. Bauer, P. Baumeister, P. F. Bornemann, J. Bouaziz, S. Brinker, J. Chico, P. H. Dederichs, B. H. Drittler, F. Dos Santos, M. dos Santos Dias, N. Essing, I. Klepetsanis, A. Kosma, N. H. Long, S. Lounis, P. Mavropoulos, E. Mendive Tapia, C. Oran, N. Papanikolaou, E. Rabel, B. Schweglinghaus, N. Stefanou, A. R. Thiess, R. Zeller, B. Zimmermann, and S. Blügel, *JuDFT-team/JuKKR: v3.6; v3.6* (2022).
- [76] J. P. Perdew, J. A. Chevary, S. H. Vosko, K. A. Jackson, M. R. Pederson, D. J. Singh, and C. Fiolhais, Atoms, molecules, solids, and surfaces: Applications of the generalized gradient approximation for exchange and correlation, *Phys. Rev. B* **46**, 6671 (1992).
- [77] K. Tanaka, Y. Yokoyama, and C. Hotta, Origin of biquadratic exchange interactions in a mott insulator as a driving force of spin nematic order, *Journal of the Physical Society of Japan* **87**, 023702 (2018), <https://doi.org/10.7566/JPSJ.87.023702>.
- [78] E. H. Lieb, The classical limit of quantum spin systems, in *Statistical Mechanics: Selecta of Elliott H. Lieb*, edited by B. Nachtergaele, J. P. Solovej, and J. Yngvason (Springer Berlin Heidelberg, Berlin, Heidelberg, 2004) pp. 433–446.
- [79] F. Körmann, A. Dick, T. Hickel, and J. Neugebauer, Rescaled monte carlo approach for magnetic systems: Ab initio thermodynamics of bcc iron, *Phys. Rev. B* **81**, 134425 (2010).
- [80] B. L. Gyorffy, Coherent-Potential approximation for a Nonoverlapping-Muffin-Tin-Potential model of random substitutional alloys, *Phys. Rev. B Condens. Matter* **5**, 2382 (1972).
- [81] A. Jacobsson, G. Johansson, O. I. Gorbatov, M. Ležaić, B. Sanyal, S. Blügel, and C. Ertz, Efficient parameterisation of non-collinear energy landscapes in itinerant magnets, *Scientific Reports* **12**, 18987 (2022).
- [82] R. Singer, F. Dietermann, and M. Fähnle, Spin interactions in bcc and fcc fe beyond the heisenberg model, *Phys. Rev. Lett.* **107**, 017204 (2011).
- [83] A. J. Freeman, O. N. Mryasov, D. S. Wang, and R. Wu, Density functional theory of the electronic and magnetic properties of interfaces and multilayers, *Mater. Sci. Eng. B* **31**, 225 (1995).
- [84] D. Spišák and J. Hafner, Theory of bilinear and biquadratic exchange interactions in iron: Bulk and surface, *J. Magn. Magn. Mater.* **168**, 257 (1997).
- [85] X. He, N. Helbig, M. J. Verstraete, and E. Bousquet, Tb2j: A python package for computing magnetic interaction parameters, *Computer Physics Communications* **264**, 107938 (2021).
- [86] M. dos Santos Dias, S. Brinker, A. Lászlóffy, B. Nyári, S. Blügel, L. Szunyogh, and S. Lounis, Reply to “comment on ‘proper and improper chiral magnetic interactions’”, *Phys. Rev. B* **105**, 026402 (2022).
- [87] J. W. Lynn, Temperature dependence of the magnetic excitations in iron, *Phys. Rev. B Condens. Matter* **11**, 2624 (1975).
- [88] T. Ozaki, Variationally optimized atomic orbitals for large-scale electronic structures, *Phys. Rev. B Condens. Matter* **67**, 155108 (2003).
- [89] T. Ozaki and H. Kino, Numerical atomic basis orbitals from H to kr, *Phys. Rev. B Condens. Matter* **69**, 195113 (2004).
- [90] M. A. Ruderman and C. Kittel, Indirect exchange coupling of nuclear magnetic moments by conduction electrons, *Phys. Rev.* **96**, 99 (1954).
- [91] T. Kasuya, A theory of metallic ferro- and antiferromagnetism on zener’s model, *Progr. Theoret. Phys.* **16**, 45 (1956).
- [92] K. Yosida, Magnetic properties of Cu-Mn alloys, *Phys. Rev.* **106**, 893 (1957).